Article

pubs.acs.org/Biomac

Sequence Effects of Self-Assembling MultiDomain Peptide Hydrogels on Encapsulated SHED Cells

Marci K. Kang,[†] John S. Colombo,[†,‡] Rena N. D'Souza,[‡] and Jeffrey D. Hartgerink*[,†,§]

Departments of [†]Chemistry and [§]Bioengineering, Rice University, Houston, Texas 77005, United States

[‡] School of Dentistry, University of Utah, Salt Lake City, Utah 84112, United States

Supporting Information

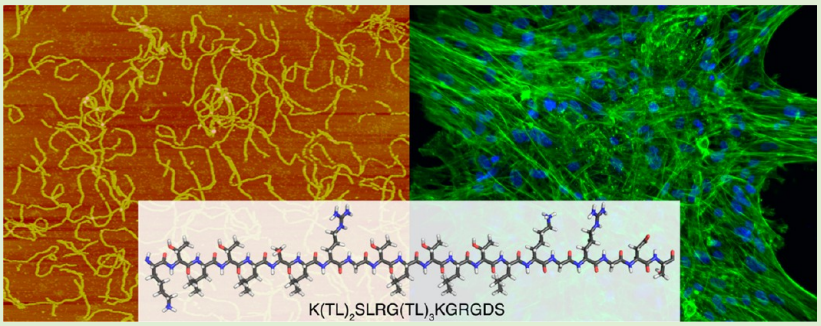

ABSTRACT: Here we report three new nanofibrous, self-assembling multidomain peptide (MDP) sequences and examine the effect of sequence on the morphology and expansion of encapsulated Stem cells from Human Exfoliated Deciduous teeth (SHED). We modified our previously reported set of serine-based MDPs, changing the serine residues in the amphiphilic region to threonine. The three new threonine-based sequences self-assemble into antiparallel β-sheet nanofibers, confirmed by CD and IR. AFM and negative-stained TEM show that the nanofibers formed by the new sequences are more curved than their serine-containing predecessors. Despite this change in nanofiber morphology, SEM illustrates that all three new sequences still form porous hydrogels. $K(TL)_2SLRG(TL)_3KGRGDS$, with a designed cleavage site, is able to be degraded by Matrix Metalloprotease 2. We then examine SHED cell response to these new sequences as well as their serine-based predecessors. We observe faster cell attachment and spreading in hydrogels formed by $K_2(SL)_6K_2GRGDS$ and $K(SL)_3RG(SL)_3KGRGDS$. By day 3, the SHEDs in all of the serine-based sequences exhibit a fibroblast-like morphology. Additionally, the SHED cells expand more rapidly in the serine-based gels while the cell number remains relatively constant in the threonine-based peptides. In hydrogels formed by $K_2(TL)_6K_2GRGDS$ and $K(TL)_2SLRG(TL)_3KGRGDS$, this low expansion rate is accompanied by changes in morphology where SHEDs exhibit a stellate morphology after 3 days in culture; however, by day 7 they appear more fibroblast-shaped. Throughout the duration of the experiment, the SHED cells encapsulated in the $K_2(TL)_6K_2$ hydrogels remain rounded. These results suggest that the basic MDP structure easily accommodates modifications in sequence and, for SHED cells, the threonine-containing gels require the integrin-binding RGDS sequence for cell attachment to occur, while the serine-based gels are less selective and support an increase in cell number, regardless of the presence or absence of RGDS.

INTRODUCTION

Self-assembling structures are frequently used as cell scaffolds because they mimic the structure and function of nature's scaffold, the extracellular matrix. Peptides that self-assemble into β-sheet nanofibers are a particularly promising class of these biomimetic materials,[1−5] one of which is now commercially available as PuraMatrix.[6−9] Most of these peptide assemblers utilize an alternating hydrophilic−hydrophobic amino acid motif to create an amphiphilic structure and thereby drive β-sheet self-assembly. This basic structure tolerates numerous modifications to the peptide sequence, which are an important method of probing the mechanism of self-assembly and surveying the sequence−structure relationship.[10−12] These peptide systems have been shown to assemble into hydrogels under physiological conditions and support 3D cell growth.[13,14] β-Sheet forming peptide hairpins that self-assemble as a function of pH have been developed that demonstrate shear thinning capabilities and can be photopolymerized to form more robust hydrogels.[15−19] Related peptides have been shown to have antibacterial and anticancer activity[20,21] and can be used as immune adjuvants.[22−24]

Our lab has developed MultiDomain Peptides (MDPs),[25] which share many of the characteristics of the above-mentioned β-sheet peptide systems. The base MDP sequence contains an alternating hydrophilic−hydrophobic region flanked by charged regions. The central amphiphilic domain drives β-sheet formation as well as nanofiber self-assembly, while the charged domain increases peptide solubility, limits the length of the

Received: January 16, 2014
Revised: April 27, 2014
Published: May 12, 2014

nanofibers by introducing molecular frustration, and provides control over the degree of self-assembly and the environment in which it takes place. For example, the charged domains also allow the resulting nanofibers to be cross-linked upon the addition of oppositely charged multivalent salts.[25]

Our first MDP, $K_2(QL)_6K_2$, formed short linear nanofibers and, upon the addition of phosphate salts, formed a hydrogel.[25] Modification of the original sequence by changing the hydrophilic amino acid to serine produced $K_2(SL)_6K_2$.[26] This sequence formed nanofibers of a similar morphology, but longer length than its glutamine-containing counterpart. Additionally, the serine-based hydrogel was able to undergo shear thinning and shear recovery, which allows the hydrogel to be loaded into a needle and delivered by injection, which was not possible with the glutamine-based system. We also examined the effect of modifying the amino acids in the charged domain, creating $E(SL)_6E$, which can be cross-linked with positively charged divalent cations such as Ca^{2+} or Mg^{2+}, but still exhibits many of the same properties as its positively charged predecessors. The hydrophobic amino acid can also be modified by introducing aromatic amino acids in the hydrophobic domain such as phenylalanine, tyrosine, and tryptophan.[27] While Leu- and Phe-based nanofibers pack in an antiparallel fashion, the use of tyrosine or tryptophan was found to result in parallel β-sheet nanofibers. These nanofibers, however, do not form robust hydrogels.

Modifications to the MDP sequence are not limited to switching out the amino acids in the base sequence. Bioactive sequences similar to those that have been previously used to selectively control cell adhesion and proliferation, can be easily incorporated into the MDP structure.[28] $K_2(SL)_6K_2$GRGDS and $K(SL)_3RG(SL)_3$KGRGDS, both of which contain the integrin-binding sequence RGDS and the latter of which incorporates SLRG, an enzyme-cleavable sequence recognized by matrix metalloprotease-2 (MMP2), have been prepared. These modifications resulted in hydrogels that retained the structural and rheological characteristics of the simpler MDP while adding bioactive functionality.[29] $K(SL)_3RG(SL)_3$KGRGDS was further examined as a cell scaffold to aid in the formation of a functional synthetic dental pulp by loading the hydrogel with growth factors and dental pulp stem cells (DPSCs).[29] These experiments demonstrated that it is possible to use MDP hydrogels as a scaffold to form vascularized tissue similar to native tissue. However, no long-term experiments have been performed to determine the effect of all of these sequence modifications on cell response.

Nanofibrous self-assembling multidomain peptides (MDPs) have also been used as a matrix for Stem cells from Human Exfoliated Deciduous teeth (SHEDs).[29,30] SHEDs[31] are a mesenchymal progenitor cell population isolated from human deciduous teeth and are an appropriate cell type to test the cytocompatibility of the MDPs, particularly as our long-term goals include dental pulp regeneration.

Herein, we report three new MDP sequences and examine how the incorporation of bioactive sequences and the modification of the hydrophilic amino acids affect cell morphology and cell number over time. We demonstrate that altering the chemistry of the MDP sequence changes SHED response to the encapsulating hydrogel. More specifically, encapsulating SHEDs in serine-based MDP hydrogels results in significant cell expansion, while the cells in the threonine-based sequences undergo morphological changes but appear to have reduced proliferation. Our results suggest that threonine-based scaffolds present a more selective matrix for cell adhesion and expansion, while serine-based scaffolds more ubiquitously promote cell expansion, regardless of the bioactive sequence.

EXPERIMENTAL SECTION

Multidomain Peptide Synthesis. All MDPs were synthesized on a low loading Rink Amide MBHA resin using an automated synthesizer with protocols previously reported by our lab.[25,32] The crude peptides were dissolved in Milli-Q water and the resulting solutions were dialyzed. $K_2(SL)_6K_2$ and $K_2(TL)_6K_2$ were dialyzed using 100−500 Da cutoff bags, $K_2(SL)_6K_2$GRGDS and $K_2(TL)_6K_2$GRGDS using 1000 Da cutoff bags and $K(SL)_3RG(SL)_3$KGRGDS and $K(TL)_2SLRG(TL)_3$KGRGDS using 2000 Da cutoff bags. Each peptide solution was dialyzed against Milli-Q water for 3 days, during which the dialysis water was refreshed twice daily. Postdialysis the peptide was lyophilized yielding a white peptide powder. MALDI-TOF mass spectrometry was performed on a Bruker Autoflex II spectrometer to characterize the purified peptides.

IR. The lyophilized peptide was dissolved in Milli-Q water and 10 μL of this solution was pipetted onto a "Golden Gate" diamond ATR-FT-IR and allowed to dry under nitrogen for a few hours. A Jasco660 IR was then used to measure the absorbance from 400 to 4000 cm^{-1}, 32 accumulations were taken per spectrum.

CD. All CD data was collected on a Jasco J-810 spectropolarimeter. Lyophilized peptide was dissolved in Milli-Q water to make a 0.01% by weight solution near pH 7. Data was collected at room temperature from 180 to 250 nm using a 0.01 cm quartz cuvette. Molar residual ellipticity (MRE) was calculated using ellipticity in millidegrees (θ), path length in cm (l), molecular weight in g/mol (m), peptide concentration in mg/mL (c), and number of residues (n_r). $MRE = (\theta \times m) \div (10 \times c \times l \times n_r)$.

AFM. Samples ranging from 0.001 to 1% by weight were prepared and imaged. For nongelled samples, the peptide was dissolved in Milli-Q water at a known concentration, pH adjusted to approximately pH 7, then the resulting solution was spin-coated onto freshly cleaved mica discs using a Headway Research photoresist spinner. A total of 5 μL of peptide solution was drop cast on the mica surface, allowed to dry for 5 s, and then washed with Milli-Q water for 10 s to remove any salt crystals, after which it was spun dry for 10 min. The sample was then imaged in tapping mode using a Digital Instruments Nanoscope IIIa.

Gelled samples were prepared by mixing a 2% by weight peptide solution with an equal volume of pH 7.4 2× phosphate buffered saline (PBS; Life Technologies, Grand Island, NY) to form a hydrogel. The introduction of phosphate buffer to form a hydrogel is the only difference between the nongelation condition and gelation condition sample preparation. The resulting 1% by weight hydrogel was then diluted with Milli-Q water to create suspensions that contained 0.001−1% peptide by weight. Each suspension was then deposited on a freshly cleaved mica disc and spin-coated using the same protocol as the nongelled samples.

Negative Stained TEM. A 2% by weight solution of phosphotungstic acid (PTA) was prepared at pH 7 and syringe filtered through a 1.0 μm filter before use. A total of 10 μL of peptide solution was pipetted onto a Quantifoil R1.2/1.3 holey carbon mesh copper grid and allowed to sit for 1 min. Afterward, the excess solution was wicked away, and the grid was inverted onto a pool of the prepared PTA solution for 10 min. The grid was removed from the solution and allowed to dry overnight before imaging. Imaging was performed using either a JEOL 1230 high contrast transmission electron microscope at 80 kV or a JEOL 2010 TEM at 200.0 kV.

Oscillatory Rheology. All rheological studies were performed on a TA Instruments AR-G2 rheometer. 200 μL of prepared hydrogel was deposited onto the rheometer stage using either a spatula or a cutoff pipet tip. Oscillatory rheology with an 12 mm stainless steel parallel plate was used with a 250 μm gap height. Strain sweep experiments were performed at a frequency of 1 rad/s from 0.001 200% strain.

Enzymatic Degradation. $K(TL)_2SLRG(TL)_3$KGRGDS was dissolved in Milli-Q water to make a 0.02% by weight solution.

MMP2 was reconstituted in Hank's buffered saline solution (HBSS; Life Technologies) to create a 0.0002% by weight solution. A total of 50 μL of the MMP2 solution was combined with 50 μL of the peptide solution and the resulting solution was placed in the incubator at 5% CO_2 and 37 °C for 24 h. The solution was then removed from the incubator and analyzed using MALDI-TOF mass spectrometry.

SEM. Lyophilized peptide was dissolved in Milli-Q water to make a 2% by weight solution. A total of 125 μL of this solution was mixed with 125 μL of 2× Dulbecco's phosphate-buffered saline (DPBS; Life Technologies) to form a 1% by weight hydrogel. The 100 μL aliquots of the resulting hydrogel were allowed to sit overnight at 4 °C. The samples were then dehydrated using a 30% ethanol to 100% ethanol gradient over a 9 h time period. The dehydrated hydrogels were then critical point dried using a critical point drier (Electron Microscopy Sciences EMS 850). The dried samples were attached to SEM pucks using conductive carbon tape and sputter coated with 7−8 nm of gold using a Denton Desk V Sputter system. All samples were imaged using a JEOL 6500F scanning electron microscope.

Cell Culture. Stem cells from human exfoliated deciduous teeth (SHEDs) were generously gifted by the Shi lab at the University of Southern California.[31] The cells were cultured in 75 cm^2 tissue culture treated flasks at 5% CO_2 and 37 °C. Cells were obtained and seeded at 3.0 × 10^5 cells/flask and cultured until they reached 70−80% confluence. Once the cells expanded sufficiently, they were incubated with Trypsin-EDTA (Life Technologies) to remove them from the flask surface and suspended in 10 mL complete media. Complete media for the SHEDs is α-MEM with 10% fetal bovine serum, 1% of 500 μg/mL L-ascorbic acid 2-phosphate, and 1% of 5000 U/mL penicillin-streptomycin (all from Life Technologies). This solution was centrifuged at 1300*g* for 6 min to pellet the cells. The media was aspirated and then the cell pellet was resuspended in HBSS to a final volume of 1 mL. A total of 10 μL of this solution was mixed with 190 μL of Trypan blue (Sigma-Aldrich, St. Louis, MO) to distinguish live cells from dead cells and to facilitate cell counting. Cells were counted using a hemocytometer and the concentration of cells/mL was calculated. Cells were seen to be greater than 95% viable. Based on the calculated number, cells were seeded in the tissue culture flasks at 3.0 × 10^5 cells/flask.

Cell Culture in Gels. SHED cells were detached and suspended in HBSS at 1.0 × 10^6 cells/mL. A total of 2% by weight peptide solutions were prepared by dissolving 10 mg of peptide in 500 μL of 298 mM sucrose (Sigma-Aldrich). The cell suspension was mixed in equal volume with the 2% by weight peptide solution to encapsulate the cells in a hydrogel. A 100 μL aliquot of this hydrogel was then pipetted into a well of a 16-well slide. Two gels were prepared per condition, per time point. Once all of the gels were aliquoted into the well slide, the slide was placed in the incubator for 30 min to ensure that the gel set. After this incubation period, 200 μL of complete growth media was gently pipetted onto the top of each gel. The complete growth media used for cell culture in gels did not contain phenol red, but was otherwise identical in composition to the media described above. This media was refreshed daily.

Confocal Microscopy. Prior to imaging, gels were washed three times with 1× PBS then fixed in 10% formalin (Fisher Scientific, Pittsburgh, PA) for 1 h. The formalin solution was removed and a solution of 0.5% Triton X (Sigma-Aldrich) in 1× PBS was applied for 15 min. The overall gel structure was maintained despite the addition of Triton-X, most likely due to covalent cross-linking as a result of media[33] and 10% formalin exposure. After 15 min the Triton X solution was removed and replaced with a 100 mM glycine (Fisher Scientific) in 1× PBS solution for 10 min. The glycine solution was then removed and 1% bovine serum albumin (BSA; Life Technologies) in PBS was added for 30 min. The BSA solution was then removed and the Alexa488-phalloidin solution (Life Technologies) was added and allowed to sit overnight. The gels were then washed three times with 1× PBS, after which the ProLong Gold with DAPI solution (Life Technologies) was applied and allowed to sit overnight. The following day the gels were removed from the well-slide and placed in a 6- or 12-well plate and submerged in 1× PBS overnight. For imaging, the gels were removed from the PBS, placed on a glass coverslip, and imaged using a Nikon A1-Rsi confocal system.

Imaging encapsulated cells in a hydrogel is difficult due to the background fluorescence of the hydrogels. In an attempt to optimize staining to minimize background fluorescence, we tried two different actin stains: Alexa488-phalloidin and Alexa568-phalloidin (Life Technologies). We found that the Alexa488-phalloidin worked better with our system so we used it for all subsequent staining. The fluorescent stains were also allowed to sit on the gels overnight to ensure that the solutions diffused all the way through the hydrogel. Additionally, allowing the stained gels to sit overnight in PBS improved the quality of the staining, possibly by washing off any nonspecifically associated stain that may have remained trapped in the gel.

Assessment of Cell Number. For each time-point and condition, cell counts were obtained by collecting five images from each of the two hydrogel constructs. The five images were selected by imaging the upper left, upper right, lower right, and lower left corners of the hydrogel, with the imaging box arranged such that the entire window was filled with hydrogel. The fifth image was obtained by placing the imaging window as close to the center of the gel as possible. The *z*-thickness for each image was held constant at 40 μm. The *z*-stack was converted into a single image using the extended depth of focus (EDF) feature in NIS-Elements. Cells were counted using ImageJ.[34] The cell counts were averaged, and for each time-point, the mean for each condition was plotted as cells/100 μL of gel. Since the cells are evenly distributed throughout the hydrogel, this calculation is valid (SI, Figure 12). Analysis of variance (ANOVA) and Tukey's test were used to determine significant differences between the different conditions.

Cell Viability. Cell viability was calculated using the same images and methodology used for cell number assessment: nuclei surrounded by actin were counted as viable, while all other nuclei were considered to be dead cells. Previous work has demonstrated a correlation between altered actin staining and a decrease in cell viability, supporting this counting methodology.[35,36] For each image, the number of viable cells was divided by the total number of cells counted, resulting in a percent viability. This percentage was averaged for each time point, and condition and standard error of the mean was calculated.

RESULTS AND DISCUSSION

TL-Series Characterization. The TL-series of peptides were synthesized using solid-phase peptide synthesis (Table 1).

Table 1. Peptides Studied

number	sequence[a]
1	$K_2(SL)_6K_2$
2	$K_2(SL)_6K_2$GRGDS
3	$K(SL)_3RG(SL)_3$KGRGDS
4	$K_2(TL)_6K_2$
5	$K_2(TL)_6K_2$GRGDS
6	$K(TL)_2SLRG(TL)_3$KGRGDS

[a]All peptides were N-terminally acetylated and C-terminally amidated.

Each of the three sequences was characterized using the same methods; for the sake of succinctness, we will primarily discuss **6**. The characterization of the other two sequences can be found in the Supporting Information (SI, Figures 4−8). For **6**, the IR spectra suggests that in the dried state the peptide forms a β-sheet, due to a peak near 1622 cm^{-1} (Figure 1A). Complementarily, the CD spectra (Figure 1B) exhibits a maximum near 195 nm and a minimum near 215 nm, both of which are indicative of β-sheet formation. These results are similar to what we have reported for the serine-based and glutamine-based MDPs.[25−27,30,32]

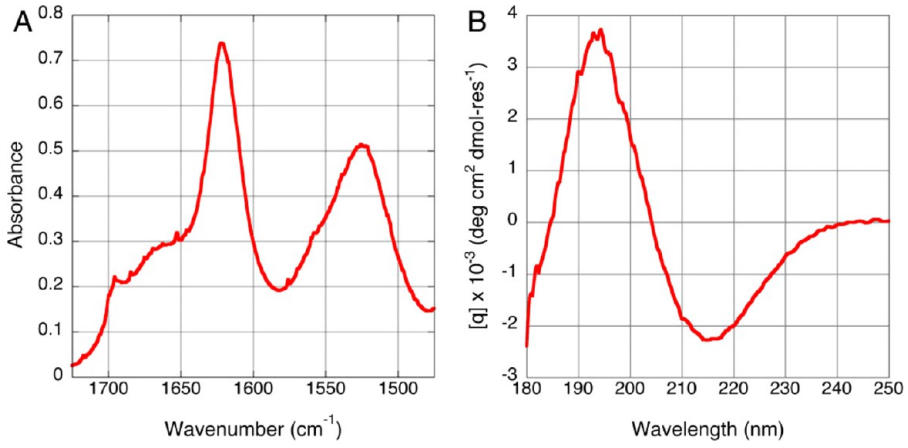

Figure 1. IR (A) and CD (B) confirm that threonine-containing MDPs form β-sheets when dried as a film and in solution, respectively.

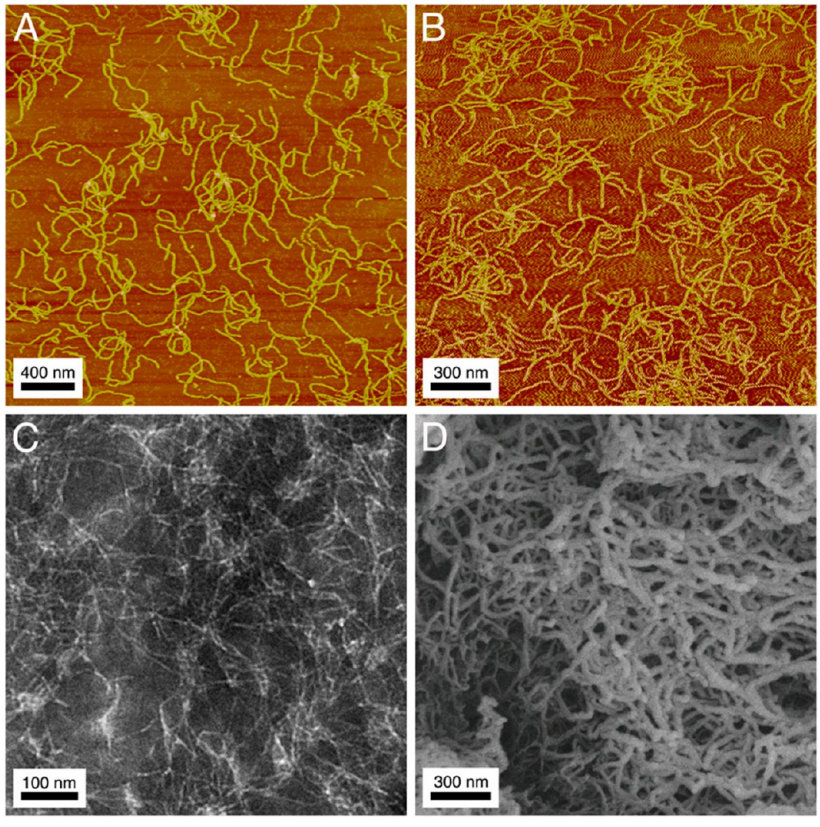

Figure 2. AFM of a 0.01% by weight peptide solution under nongelation conditions (A) and gelation conditions (B); TEM of a 0.01% by weight peptide solution under nongelation conditions (C); and SEM of 1% by weight hydrogel (D) of $K(TL)_2SLRG(TL)_3KGRGDS$ nanofibers illustrate the different morphology observed with the TL-based nanofibers.

As with the previously characterized MDP sequences, nanofiber formation was confirmed using atomic force microscopy (AFM) and transmission electron microscopy (TEM). The TL-series of peptides forms long, curved nanofibers (Figure 2A–C), which differ morphologically from the more linear, rigid appearing nanofibers formed by the previously reported MDPs. The long-range order of the hydrogel formed by **6** was assessed using scanning electron microscopy (SEM), demonstrating that when phosphate ions are introduced into the system the MDP nanofibers further self-assemble into a porous nanofibrous hydrogel (Figure 2D). Like its SL-series counterpart, **6** contains a bioactive SLRG motif, which is recognized by MMP2, allowing for the controlled degradation of the MDP.[30] The incorporation of this bioactive sequence is useful for future in vivo experiments where we want to ensure that complete proteolysis of the material is possible. The MALDI-TOF spectra (Figure 3) of MDP **6** after 48 h incubation with MMP-2 shows multiple degradation products, including one of the expected fragments: acetyl-KTLTLS. Other observed fragments can be attributed to nonspecific degradation, which was also seen by Galler et al. when **3** was incubated with MMP2, suggesting that switching to threonine in the hydrophilic face of the peptide does not affect the designed enzymatic degradation.[30]

Cytocompatibility and Sequence Comparison. The ability of a synthetic scaffold to support cells is a critical part of

dx.doi.org/10.1021/bm500075r | *Biomacromolecules* 2014, 15, 2004–2011

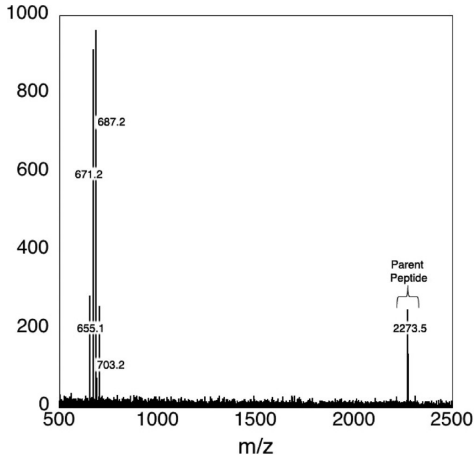

Figure 3. MALDI-TOF spectrometry of the peptide after 24 h of incubation with MMP-2 shows partial decomposition of the parent peptide including one of the expected fragments, [acetyl-KTLTLS + $H^+]^+$ (m/z = 687), as well as other fragments that suggest nonspecific degradation: [KGRGDS-amide + $K^+]^+$ (m/z = 656), and [G-$(TL)_3$KGRGDS-amide + $Na^+]^+$ (m/z = 670).

the tissue engineering triad. Ideally such a scaffold would mimic the native ECM, interacting with the cells by providing bioactive signals and promoting cell behavior such as attachment, spreading, and scaffold remodeling. Previously, we demonstrated that the SL-series of MDPs was capable of supporting cells.[29,30] After 24 h, SHEDs seeded in hydrogels of MDP **2** and **3** exhibited larger cell bodies when compared to cells seeded in hydrogels of MDP **1**, suggesting that adding the integrin-binding sequence and the enzyme-cleavable sequence positively altered cell morphology.[30] As mentioned above, we incorporated their findings when designing the TL-series of peptides, creating MDP **5** with the integrin-binding sequence and MDP **6** that combined both the integrin-binding and enzyme-cleavable sequence.

In order to investigate the long-term effect of MDP sequence on cellular response, we encapsulated SHED cells in hydrogels formed from the three new threonine-based MDPs as well as three previously reported serine-based sequences and imaged the gels after 1, 3, 7, and 11 days in culture.[26,30] Since we wanted to isolate the effect of MDP sequence on cellular response we did not include any growth factors or other biomacromolecules in the hydrogel constructs. The nanofibrous hydrogels were cultured for the predetermined period of time and then fixed and stained with Alexa488-phalloidin and DAPI in order to visualize the actin cytoskeleton and cell nuclei, respectively. Confocal images of the stained gels show that by day 1 the SHED cells spread out and extend processes in the hydrogels of MDP **2** and **3** (Figure 4E,I), but remain fairly rounded in **4**–**6** (Figure 5A,E,I). Qualitatively, it appears

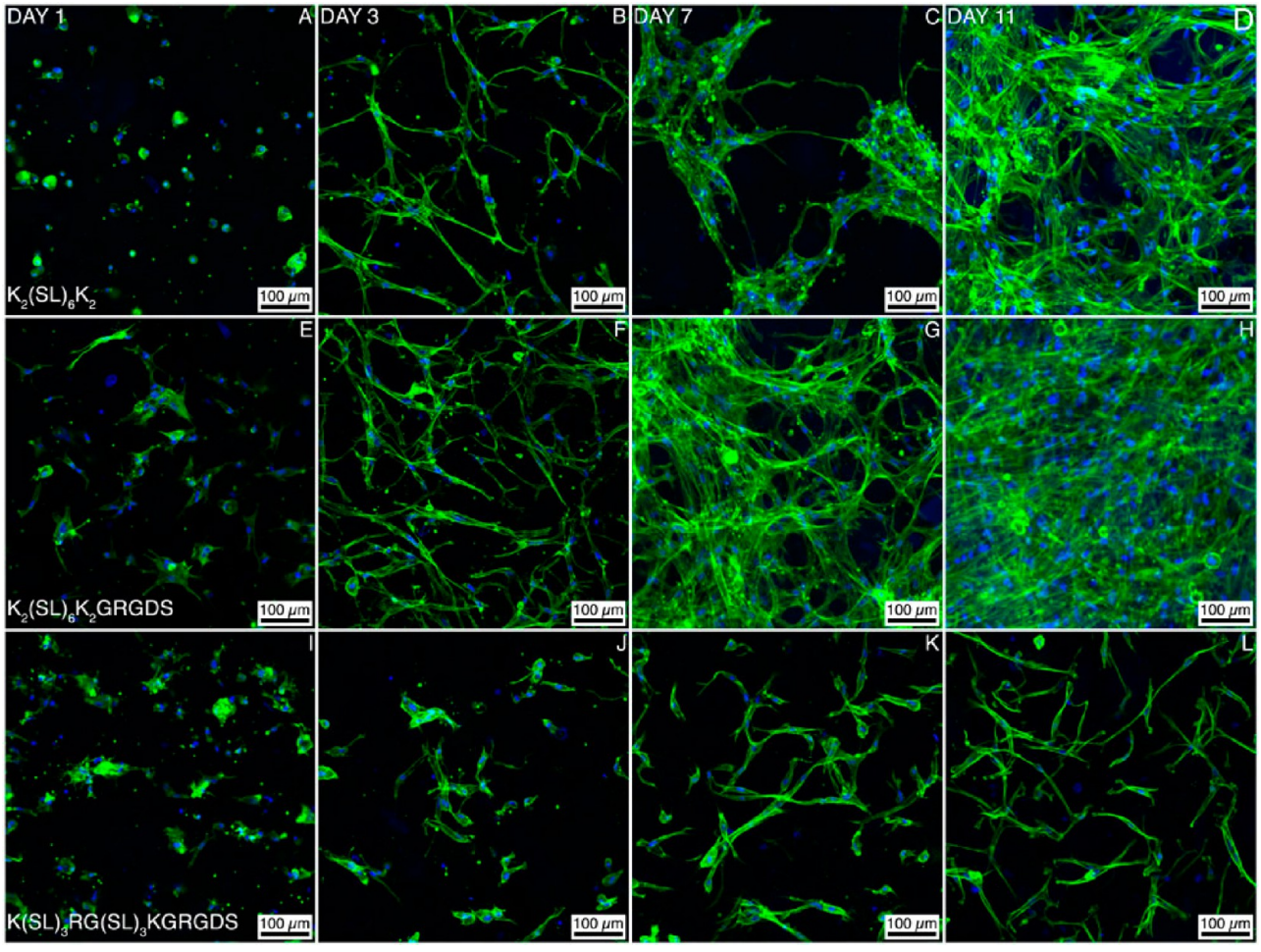

Figure 4. Confocal images of SHED cells 1, 3, 7, or 11 days after 3D encapsulation in $K_2(SL)_6K_2$ (A–D), $K_2(SL)_6K_2$GRGDS (E–H), and K$(SL)_3$RG$(SL)_3$KGRGDS (I–L) hydrogels show that SL-based scaffolds are only modestly selective and generally promote SHED expansion.

dx.doi.org/10.1021/bm500075r | *Biomacromolecules* 2014, 15, 2004–2011

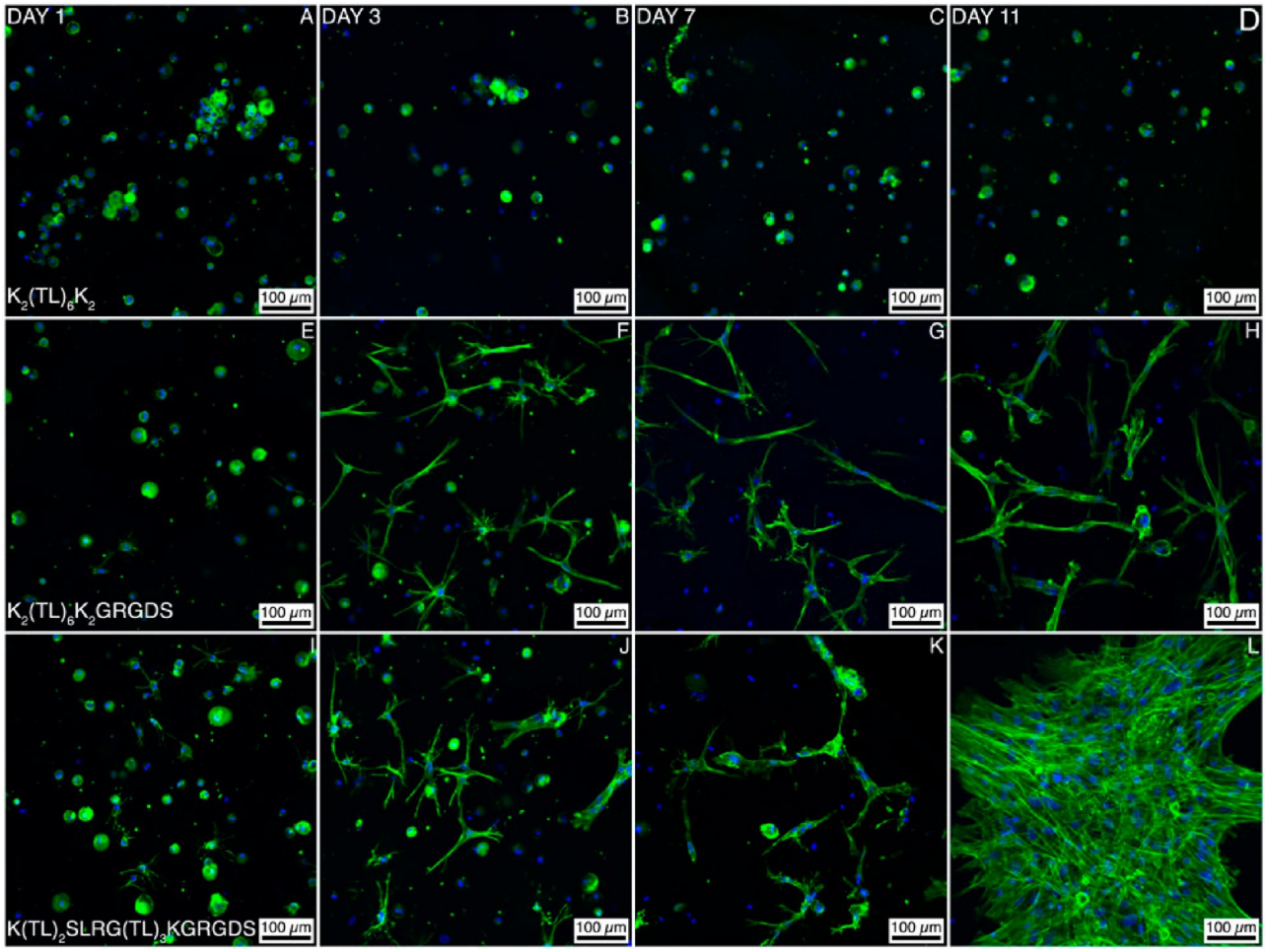

Figure 5. Confocal microscopy of SHEDs after 1, 3, 7, or 11 days after 3D encapsulation in $K_2(TL)_6K_2$ (A–D), $K_2(TL)_6K_2GRGDS$ (E–H), and $K(TL)_2SLRG(TL)_3KGRGDS$ (I–L) hydrogels.

that the SHEDs encapsulated in **2** and **3** have slightly larger cell bodies than those in **1** (Figure 4A,E,I) supporting our previous findings.[30]

After 3 days in culture, the SHEDs encapsulated in **1** and **2** extend long processes, form cell–cell interactions, and exhibit a fibroblast-like morphology (Figure 4B,F). The change is less dramatic in **3** where cell density remains similar to the earlier time point and no long, extended processes are observed (Figure 4J). No change in cell morphology is observed in the hydrogels of MDP **4** after 3 days in culture (Figure 5B). SHEDs cultured in the gels of **5** and **6** exhibit a stellate morphology, with a large, round cell body with numerous thin projections emanating from it (Figure 5F,J).

By day 7 the cells growing in **1** and **2** have begun to form porous networks of cells (Figure 4C,G). The networks formed in **1** contain denser clusters of cells with larger gaps between the clusters than those formed in **2** (Figure 4C,G and SI, Figure 9C,G). At the same time point, the SHEDs encapsulated in the hydrogels of MDPs **5** and **6** gels acquire a more fibroblast-like morphology than what was observed at the earlier time points while proliferating minimally (Figure 5G,K). Again, the cells in **4** remain rounded (Figure 5C).

After 11 days in culture, the cells invade the entirety of the hydrogels of MDP **1** and **2** and expand to fill the majority of their volume (Figure 4D,H and SI, Figure 9D,H). In MDP **3** and **5**, a slight increase in cell spreading is noted, but other than that, no change is observed compared to the day 7 time point (Figures 4L and 5H). The lack of exogenous growth factors in these scaffolds makes these materials potentially interesting from a tissue engineering standpoint, as the MDP hydrogel itself seems to be sufficient to support SHED expansion and attachment. Between days 7 and 11, the cells in MDP **6** heterogeneously fill the hydrogel, resulting in large clusters of cells in some areas and low cell density in other areas (Figure 5L and SI, Figure 10L). Since the overall cell density does not change significantly from day 7 to day 11 (see Figure 6), it is most likely that the formation of large clusters of cells arose from cell migration rather than from proliferation.

The persistent rounded morphology of the SHED cells in the hydrogels formed from MDP **4** suggests that the cells are not attaching to the surrounding nanofibrous network (Figure 5A–D). Since **4** does not contain the integrin-binding motif, this result is not unexpected. Although no morphological changes are observed, we believe that the cells in **4** are still alive as they do not exhibit the same staining patterns as encapsulated cells that we have treated with methanol (SI, Figure 11). We did not expect the cells to attach and expand well in **1**, which also does not contain an adhesion motif and only differs chemically from **4** in the addition of six methyl groups in the hydrophilic face. It is unclear why the SHEDs are able to attach and expand in the hydrogels of MDP **1** while they remain rounded in **4**.

dx.doi.org/10.1021/bm500075r | *Biomacromolecules* 2014, 15, 2004–2011

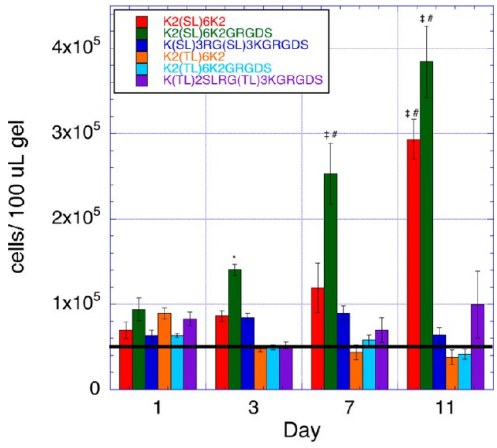

Figure 6. Cell density by sequence over time shows that SHEDs expand rapidly in $K_2(SL)_6K_2GRGDS$ hydrogels. Symbols indicate the following: #, significant compared to its value at the previous time point; ‡, significant compared to all other sequences at the same time point; * significant compared to $K_2(TL)_6K_2$ and $K_2(TL)_6K_2GRGDS$ at the same time point. Table of *p*-values can be found in the Supporting Information.

The confocal data demonstrates that the chemistry of the hydrogel can have a significant effect on encapsulated SHED cells. Even though chemically MDP **1** and **4** differ only by six methyl groups the SHED cells do not adhere and expand poorly in MDP **4**, but thrive in **1**. In the serine-based sequences the presence of the RGDS motif encourages early cell attachment and spreading, but at later time points is not required for cell spreading and expansion. This is not the case for the threonine-based sequences, in which lack of RGDS results in rounded cell morphology at all time points, suggesting that the threonine sequences are more selective than the serine-based MDPs. While it is possible that hydrogel mechanics play a role in altering cellular response, it seems unlikely as **2**, **3**, and **5** have similar G' values yet elicit different cell responses (Table 2).

Table 2. Storage Modulus (G') of Studied Peptides

number	sequence	G' (Pa)
1	$K_2(SL)_6K_2$	400[30]
2	$K_2(SL)_6K_2GRGDS$	150[30]
3	$K(SL)_3RG(SL)_3KGRGDS$	175[30]
4	$K_2(TL)_6K_2$	80
5	$K_2(TL)_6K_2GRGDS$	140
6	$K(TL)_2SLRG(TL)_3KGRGDS$	63

Figure 6 quantifies the degree of cell expansion in each type of hydrogel over time. Cell density is approximately the same in each type of hydrogel on day 1. By day 3 the cell density in the SL-based hydrogels increases, dramatically in the case of MDP **2**, while the density does not change significantly in the TL-hydrogels. The SHEDs in the SL-hydrogels continue to expand from day 3 to day 7, showing a significant increase in the hydrogels of **2**. No significant change is observed in the TL-based hydrogels, which retain roughly the same cell density for the remainder of the experiment. Interestingly, although cell viability decreases in MDPs **4**–**6** over time (SI, Figure 13), there is no significant change observed in cell density, suggesting that the rate of cell proliferation is similar to that of apoptosis. From day 7 to day 11, the cell density changes significantly in the **1** and **2** hydrogels, and it is unclear as to what causes the sudden increase in the population of MDP hydrogel **1**. However, it is possible that the production of native collagen and fibronectin may allow the initially unfavorable chemical environment to become more conducive to cell proliferation after day 7. These results suggest that the threonine-containing hydrogels are more selective, requiring the RGDS sequence for cell attachment to occur, while the serine-based sequences are more proliferative and will support large increases in cell population even if bioactive sequences are not present.

CONCLUSIONS

We have shown that the MDP design is flexible and can tolerate a substitution in the hydrophilic face as well as the addition of multiple bioactive sequences. The three new sequences form β-sheet nanofibers confirmed by CD and IR. AFM and TEM show that the nanofibers exhibit a curved morphology, which differs from the more rigid, previously characterized SL-series of peptides.[26,30] SEM illustrates that the addition of phosphate salts results in a porous nanofiber network similar to that formed by the serine-based MDPs. MALDI-TOF spectrometry of **6** that has been incubated with MMP-2 overnight indicates that the peptide can be degraded by the enzyme allowing for the possibility of scaffold remodeling similar to what occurs in native ECM.

The encapsulation of SHED cells in the scaffolds shows that the different sequences have varying effects on cell morphology and expansion. All sequences exhibit some cytocompatibility, but the threonine-based MDPs are more dependent on bioactive functionalization for cell attachment to occur. Cells were seen to attach and expand in the serine-based gels despite the lack of encapsulated growth factors such as TGF-β and FGF-2, a finding that we consider to be significant. SHEDs exhibit more rapid attachment and process formation in the SL-based hydrogels, adopting a fibroblast-like morphology by day 3 in **1** and **2** and day 7 in **3**. By day 3, in the threonine-containing hydrogels, the SHEDs exhibit a stellate morphology displaying rounded cell bodies with thin projections. At day 7, this morphology has disappeared and the cells take on a fibroblast-like morphology. By the final time point, the SHEDs expand to form large networks of cells throughout the **1** and **2** hydrogels and large colonies of cells in the **6** hydrogels. The findings reported here highlight the importance of screening scaffolds with cells as minor changes in the peptide sequence can significantly alter cellular responses to the scaffold. Additionally, the innate compatibility of the SL-based sequence with SHED cells suggests a possible use of the scaffolds in oral tissue regeneration.

ASSOCIATED CONTENT

Supporting Information

Additional material characterization including mass spectra, IR, AFM, TEM, rheology, and confocal microscopy. This material is available free of charge via the Internet at http://pubs.acs.org.

AUTHOR INFORMATION

Corresponding Author

*E-mail: jdh@rice.edu.

Notes

The authors declare no competing financial interest.

■ ACKNOWLEDGMENTS

This work was funded by the Robert A. Welch Foundation (Grant No. C1557) and the NIH (R01 DE021798-01A1).

■ REFERENCES

(1) Jung, J. P.; Gasiorowski, J. Z.; Collier, J. H. *J. Pept. Sci.* **2010**, *94*, 49−59.
(2) Bowerman, C. J.; Nilsson, B. L. *Biopolymers* **2012**, *98*, 169−184.
(3) Webber, M. J.; Tongers, J.; Newcomb, C. J.; Marquardt, K. T.; Bauersachs, J.; Losordo, D. W.; Stupp, S. I. *Proc. Natl. Acad. Sci. U.S.A.* **2012**, *109*, 9220.
(4) Matson, J. B.; Stupp, S. I. *Chem. Commun.* **2012**, *48*, 26−33.
(5) Maude, S.; Ingham, E.; Aggeli, A. *Nanomedicine* **2013**, *8*, 823−847.
(6) Holmes, T. C.; de Lacalle, S.; Su, X.; Liu, G. S.; Rich, A.; Zhang, S. G. *Proc. Natl. Acad. Sci. U.S.A.* **2000**, *97*, 6728−6733.
(7) Kisiday, J.; Jin, M.; Kurz, B.; Hung, H.; Semino, C.; Zhang, S.; Grodzinsky, A. J. *Proc. Natl. Acad. Sci. U.S.A.* **2002**, *99*, 9996−10001.
(8) Zhang, S. G.; Holmes, T. C.; Dipersio, C. M.; Hynes, R. O.; Su, X.; Rich, A. *Biomaterials* **1995**, *16*, 1385−1393.
(9) Nagai, Y.; Unsworth, L. D.; Koutsopoulos, S.; Zhang, S. G. *J. Controlled Release* **2006**, *115*, 18−25.
(10) Bowerman, C. J.; Ryan, D. M.; Nissan, D. A.; Nilsson, B. L. *Mol. Biosyst.* **2009**, *5*, 1058−1069.
(11) Bowerman, C. J.; Liyanage, W.; Federation, A. J.; Nilsson, B. L. *Biomacromolecules* **2011**, *12*, 2735−2745.
(12) Wang, K.; Keasling, J. D.; Muller, S. J. *Int. J. Biol. Macromol.* **2005**, *36*, 232−240.
(13) Kyle, S.; Aggeli, A.; Ingham, E.; McPherson, M. J. *Biomaterials* **2010**, *31*, 9395−9405.
(14) Maude, S.; Miles, D. E.; Felton, S. H.; Ingram, J.; Carrick, L. M.; Wilcox, R. K.; Ingham, E.; Aggeli, A. *Soft Matter* **2011**, *7*, 8085−8099.
(15) Schneider, J. P.; Pochan, D. J.; Ozbas, B.; Rajagopal, K.; Pakstis, L.; Kretsinger, J. *J. Am. Chem. Soc.* **2002**, *124*, 15030−15037.
(16) Giano, M. C.; Pochan, D. J.; Schneider, J. P. *Biomaterials* **2011**, *32*, 6471−6477.
(17) Nagy, K. J.; Giano, M. C.; Jin, A.; Pochan, D. J.; Schneider, J. P. *J. Am. Chem. Soc.* **2011**, *133*, 14975−14977.
(18) Haines-Butterick, L.; Rajagopal, K.; Branco, M.; Salick, D.; Rughani, R.; Pilarz, M.; Lamm, M. S.; Pochan, D. J.; Schneider, J. P. *Proc. Natl. Acad. Sci. U.S.A.* **2007**, *104*, 7791−7796.
(19) Yan, C. Q.; Mackay, M. E.; Czymmek, K.; Nagarkar, R. P.; Schneider, J. P.; Pochan, D. J. *Langmuir* **2012**, *28*, 6076−6087.
(20) Veiga, A. S.; Sinthuvanich, C.; Gaspar, D.; Franquelim, H. G.; Castanho, M. A. R. B.; Schneider, J. P. *Biomaterials* **2012**, *33*, 8907−8916.
(21) Sinthuvanich, C.; Veiga, A. S.; Gupta, K.; Gaspar, D.; Blumenthal, R.; Schneider, J. P. *J. Am. Chem. Soc.* **2012**, *134*, 6210−6217.
(22) Jung, J. P.; Nagaraj, A. K.; Fox, E. K.; Rudra, J. S.; Devgun, J. M.; Collier, J. H. *Biomaterials* **2009**, *30*, 2400−2410.
(23) Rudra, J. S.; Tian, Y. F.; Jung, J. P.; Collier, J. H. *Proc. Natl. Acad. Sci. U.S.A.* **2010**, *107*, 622−627.
(24) Rudra, J. S.; Tripathi, P. K.; Hildeman, D. A.; Jung, J. P.; Collier, J. H. *Biomaterials* **2010**, *31*, 8475−8483.
(25) Dong, H.; Paramonov, S. E.; Aulisa, L.; Bakota, E. L.; Hartgerink, J. D. *J. Am. Chem. Soc.* **2007**, *129*, 12468−12472.
(26) Aulisa, L.; Dong, H.; Hartgerink, J. D. *Biomacromolecules* **2009**, *10*, 2694−2698.
(27) Bakota, E. L.; Sensoy, O.; Ozgur, B.; Sayar, M.; Hartgerink, J. D. *Biomacromolecules* **2013**, *14*, 1370−1378.
(28) Patel, P. N.; Gobin, A. S.; West, J. L.; Patrick, C. W. *Tissue Eng.* **2005**, *11*, 1498−1505.
(29) Galler, K. M.; Hartgerink, J. D.; Cavender, A. C.; Schmalz, G.; D'Souza, R. N. *Tissue Eng., Part A* **2012**, *18*, 176−184.
(30) Galler, K. M.; Aulisa, L.; Regan, K. R.; D'Souza, R. N.; Hartgerink, J. D. *J. Am. Chem. Soc.* **2010**, *132*, 3217−3223.
(31) Miura, M.; Gronthos, S.; Zhao, M. R.; Lu, B.; Fisher, L. W.; Robey, P. G.; Shi, S. T. *Proc. Natl. Acad. Sci. U.S.A.* **2003**, *100*, 5807.
(32) Bakota, E. L.; Wang, Y.; Danesh, F. R.; Hartgerink, J. D. *Biomacromolecules* **2011**, *12*, 1651−1657.
(33) Bakota, E. L.; Aulisa, L.; Galler, K. M.; Hartgerink, J. D. *Biomacromolecules* **2011**, *12*, 82.
(34) Schneider, C. A.; Rasband, W. S.; Eliceiri, K. W. *Nat. Methods* **2012**, *9*, 671−675.
(35) Banan, A.; Smith, G. S.; Kokoska, E. R.; Miller, T. A. *J. Surg. Res.* **2000**, *88*, 104−113.
(36) Olabarrieta, I.; L'Azou, B.; Yuric, S.; Cambar, J.; Cajaraville, M. P. *Toxicol. In Vitro* **2001**, *15*, 511−517.